A redox active rod coordination polymer from tetrakis(4-carboxylic acid biphenyl)tetrathiafulvalene

Nicolas Zigon, Federica Solano, Pascale Auban-Senzier, Stéphane Grolleau, Thomas Devic, Pavel Zolotarev, Davide Proserpio, Boleslaw Barszcz, Iwona Olejniczak, Narcis Avarvari

A redox active rod coordination polymer from tetrakis(4-carboxylic acid biphenyl)tetrathiafulvalene

Nicolas Zigon,*[,a] Federica Solano,[a] Pascale Auban-Senzier,[b] Stéphane Grolleau,[c] Thomas Devic,[c] Pavel N. Zolotarev,[d] Davide M. Proserpio,[d] Bolesław Barszcz[e],[e] Iwona Olejniczak,[e] Narcis Avarvari*[,a]

[a] Univ Angers, CNRS, MOLTECH-ANJOU, SFR MATRIX, F-49000 Angers, France. E-mail: narcis.avarvari@univ-angers.fr; nicolas.zigon@univ-angers.fr

[b] Université Paris-Saclay, CNRS, UMR 8502, Laboratoire de Physique des Solides, 91405 Orsay, France

[c] Université de Nantes, CNRS, Institut des Matériaux Jean Rouxel, IMN, F-44000 Nantes, France

[d] Università degli studi di Milano, Dipartimento di Chimica, Via Golgi 19, 20133 Milano, Italy

[e] Institute of Molecular Physics, Polish Academy of Sciences, Smoluchowskiego 17, 60-179 Poznań, Poland

Table of content

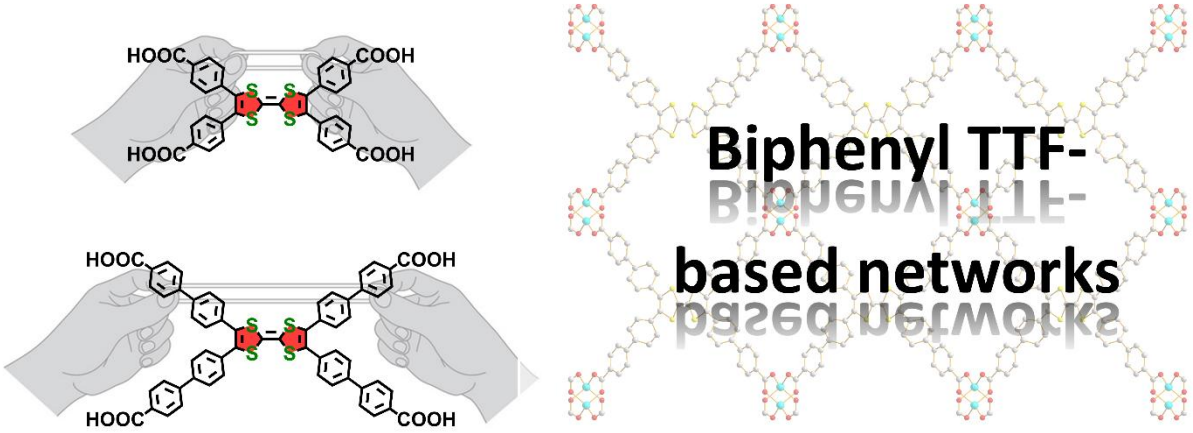

A sprawling scaffold. Tetrathiafulvalene-tetrabenzoic acid has been widely used in redox active Porous Coordination Polymers design, but the differences in the networks reported so far stands mostly on the metals or metal clusters SBUs used. Herein is reported an extension of the spacers between the redox active core and the SBUs along with the related PCP structure.

Keywords

Conductivity

Organic donors

Porous Coordination Polymer

Raman Spectroscopy

Single-crystal X-ray crystallography

Tetrathiafulvalene

Abstract

An enlarged version of the ubiquitous tetrathiafulvalene-tetrabenzoic acid is described, with 4,4'-biphenyls moieties as spacers between the coordination moieties and the electroactive core. The obtained rectangular ligand has a 14 x 22 $Å^2$ size, and is combined with Zn(II) in solvothermal conditions to yield a coordination polymer endowed with large cavities of *ca*. 15 x 11 Å² / 10 x 10 Å². The topology of the material is discussed in details using the Points of Extension and Metals (PE&M) or the Straight-rod (STR) representation, and reveals respectively the **sqc1121** or **tfo** topological type of the structure. Its stability towards solvent removal and electrical properties are discussed. The material does not present any permanent porosity upon desolvation according to nitrogen sorption measurements at 77 K. Nevertheless, a significant increase of conductivity is observed on compressed-pellets of the material upon post-synthetic oxidation with iodine. Raman spectroscopy combined with density functional theory (DFT) calculations has been used to characterize the oxidation state in the tetrakis(4-carboxylic acid biphenyl) tetrathiafulvalene for coordination polymers.

Introduction

Coordination polymers are "*coordination compounds with repeating coordination entities extending in 1, 2, or 3 dimensions*" according to the IUPAC definitions.[1] These often crystalline materials are composed of metal ions, clusters or chains coordinated by polytopic and divergent ligands. Since the first modern reports by Robson *et coll.* in the early 90s,[2,3] an intense activity strove around these novel materials, especially for promising applications in the fields of gas storage,[4–6] catalysis,[7–9] separations[10–13], single-molecule characterizations,[14–17] , high energy materials,[18] or chemical sensing.[19,20] Most of the networks described so far are not displaying a noticeable electronic conductivity because of a large HOMO/LUMO gap of the organic linkers and/or a poor orbital overlap with the metal centres.[21] While early reports described non-porous conductive coordination polymers with materials such as dicyanoquinonediimine-Cu or tetracyanoquinodimethane-Cu (σ in the 5 to $5 \cdot 10^7$ S/m range),[22–24] it is only in the late 2000s that electroactive coordination polymers were devised using pyrazine dithiolates,[25,26] benzene-hexathiolate or tetrathiafulvalene-tetracarboxylic acid as redox active ligands.[27,28] Such redox active materials – if embedded with accessible pores – are expected to find applications in electrochemical sensing,[29,30] thermoelectrics,[31] fuel cells,[32] batteries[33,34] or supercapacitors.[35–37] The redox behaviour of these materials is based on structure related charge-transport mechanisms such as through-bond,[38,39] through-space or redox hopping.[21] The tetrathiafulvalene (TTF) scaffold is widely recognized as an excellent basis for organic conductors.[40–42] Consequently, it was incorporated within coordination polymers to yield materials with Brunauer–Emmett–Teller (BET) surface areas up to 660 m^2/g and conductivities in the 10^{-8} to 10^{-1} S/m range.[28,43–48] One can still note that these values are far lower than that typically found in molecular salts, as the geometrical constrains associated to the formation of the coordination networks usually impedes an optimal orbital overlap between the TTF cores.

The workhorse for TTF-based porous coordination polymers (PCPs) is the TTF-tetrabenzoate (TTFTB) which was combined with M(II) (M = Cd, Co, Mn, Zn)[44,49] or M(III) cations (M = La, Gd, Dy, Tb, Ho, Er, Yb, Lu).[50–53] The structures with M(II) cations are all isostructural and in the $P6_5$ space group. The TTF form 1D stacks with the 6_5 screw axis slightly offset from the TTF barycentre, and S-S distances are in the 3.65-3.77 Å range. Conductivities (up to $2.9 \cdot 10^{-2}$ S/m) are anisotropic and higher along the TTF stacks. A post-synthetic oxidation with tetracyanoethylene increases the conductivity by two orders of magnitude.[54] The structures with rare earths display a broader variety, depending not only on the metal but also on the synthetic conditions. Rod-like chains of lanthanides and carboxylates are often observed, thus creating 1-D chains of TTFTB, with conductivities up to $1.5 \cdot 10^{-3}$ S/m for MUV-5a ($d_{S\text{-}S}$ = 3.61 - 3.86 Å).[51]

The PCPs containing rod secondary building units (SBU) are particularly appealing for the stacked arrangement that they impose to the organic parts, which favours through-space electron transport.[55] Furthermore, the isoreticular principles in PCP chemistry is an approach where the same framework topology is obtained from ligands with a similar connectivity and coordinating moieties, but different non-coordinating functional groups.[56] In that regard, an increase of the pore size of a conductive coordination polymer should be observed by simply expanding the distances between the coordination sites of the redox active ligand.

Herein will therefore be presented and discussed the synthesis of a novel ligand based on TTF, which is regarded as an isoreticular expansion of the TTFTB scaffold. Its combination with Zn(II) to obtain a rod PCP, along with the study of the stability and conductivity of the obtained material, will be described.

Results and discussion

The ligand **1-H$_4$** (**Figure 1**) is designed to bear 4 carboxylic acids in a divergent fashion, around a redox active tetrathiafulvalene core. Each acid moiety is separated from the TTF core by 4,4'-biphenyl spacers. **1-H$_4$** has its carboxylic acid groups separated by 14 and 22 Å along its shortest and longest side respectively. This represents an increase of *ca.* 50% of the molecule size in comparison to TTFTB (**Figure 1**), without changing significantly the size ratio between its length and width (d_{length}/d_{width} = 1.6).

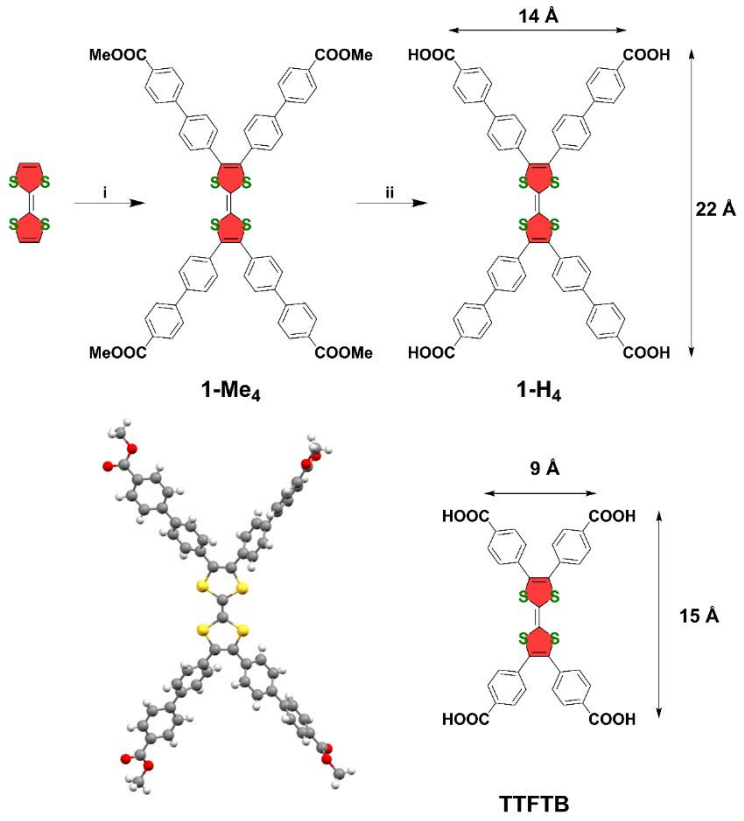

Figure 1. (top) Synthesis of the tetrakis(4-carboxylic acid biphenyl)tetrathiafulvalene ligand **1-H$_4$**. i) $Pd(OAc)_2$, Cs_2CO_3, P(*t*Bu)$_3$·HBF_4, dioxane, reflux, 79% ; ii) NaOH, THF/MeOH/H_2O, reflux, 92%. (bottom) X-ray structure of **1-Me$_4$** and representation of the analogous TTFTB.

Starting from commercial TTF, a palladium-catalysed direct C-H arylation yielded the tetra-methylester **1-Me$_4$** intermediate with a 79 % yield.[57] Saponification followed by re-acidification yielded the tetra-acid with a 92% yield at the 100 mg scale. **1-Me$_4$** crystallized in the triclinic *P*–1 space group (**Figure 1**, **see Table S1** for details). As expected for such a TTF derivative, two redox waves are observed in solution in cyclic voltammetry (**see Fig. S1**), with $E^1_{1/2}$ = 0.29 V and $E^2_{1/2}$ = 0.52 V vs. Fc^+/Fc corresponding to the successive formation of the radical cation and dication of the TTF.

The protocol described for the combination of TTFTB with Zn(II) had to be adapted to **1-H$_4$**. A solution of the title compound in dimethylacetamide was carefully layered by a solution of $Zn(NO_3)$,$6H_2O$ in EtOH in an autoclave. After 2 days at 100°C, thin red needles of **1-Zn$_2$** suitable for X-ray diffraction analysis on single crystals were obtained. Larger microcrystalline batches were obtained by multiplying by a factor 5 the concentrations, and their purity assessed by elemental analysis and powder X-ray diffraction (**see Fig. S4**).

1-Zn$_2$ crystallizes in the monoclinic *C*2/m space group, with one fourth of **1**$^{4-}$ and half a Zn(II) atom in the asymmetric unit, leading to a neutral network. Two disordered DMAc molecules with 25% occupancy each are also present. The remaining electronic density could not be attributed to any

crystallographically ordered molecule and was treated with the solvent mask function (equivalent to the SQUEEZE function of the PLATON software) of the Olex2 software.[58] Both phenyl rings are disordered over two positions with 50% occupancies on each part. Each Zn(II) metal centre stands in a tetrahedral environment, with 4 O-atoms coming from four different **1** molecules in its coordination sphere. Two Zn atoms are connected through two bridging carboxylates, thus forming an 8-membered ring. These rings connect along the *a*-axis to create an infinite metallo-organic rod as the SBU of this structure, identical to the rods first observed in MOF-77 with the difference that in our compound the rods are all parallel (**Figure 2a**).[59]

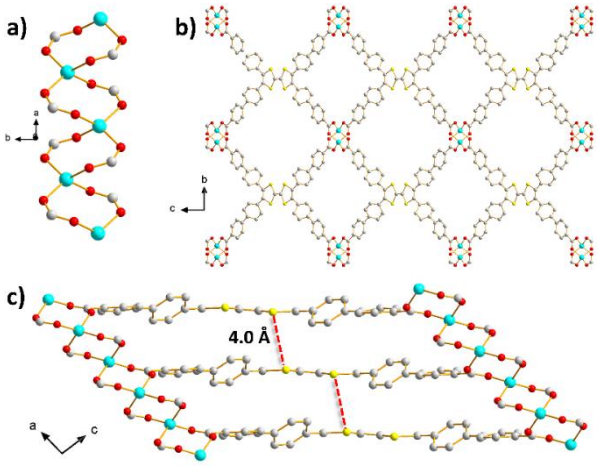

Figure 2. X-ray crystal structure for **1-Zn$_2$.** a) Infinite metal-carboxylate rods as the secondary building unit (ribbon-of-rings), b) view of the pores along the *a*-axis and c) a side view of a shifted TTF stack along the *b*-axis with the shortest intermolecular S-S distance highlighted in red (solvent molecules, disordered phenyls and H-atoms omitted for the sake of clarity, Zn : blue ; S : yellow ; O : red ; C : grey).

Thanks to the organization imposed by the pillared SBU, the TTF cores are stacked along the *a*-axis as well with interplanar distances of 4.03 Å. The TTF moieties are not eclipsed but translated by *ca.* 4.3 Å. The shortest intermolecular S-S distance at 4.0089(13) Å is too large for creating a proper band dispersion (**Figure 2c**). The central C=C bond is 1.3412(64) Å, which is in the expected length range for a non-oxidised TTF core. The dithiol-ethylene moieties are twisted of *ca*. 7.36° regarding to the central C=C bond. The phenyl rings are distorted regarding to the plane of the TTF with dihedral angles between 36 and 56° for the phenyl ring closer to the TTF core, and 3 to 27° for the phenyl ring further to the TTF core.

The networks delimits 1-D rhombus cavities occupied by solvent molecules (**Figure 2b**). Two types of parallel channels are identified, and the smallest one contains the disordered DMAc molecules. This structure is reminiscent of MUV-5,[51] or lanthanide-TTFTB coordination polymers.[52,53] In these reported cases TTF stacking sequences as dimers or trimers are observed, while in our case the TTF is

homogenously stacked. Furthermore, as expected, the size of these channels is expanded from *ca*. 12 x 5 Å² / 6.5 x 6 Å² for (Ln)TTFTB-based networks to *ca*. 15 x 11 Å² / 10 x 10 Å², in good accordance with the 50% increase due to the ligand expansion. The SQUEEZE calculations from the PLATON suite gives a total solvent accessible volume of 1492 $Å^3$ per unit cell, accounting for 40 % of the total volume.[60,61]

A better understanding of the network structure is achieved using the ToposPro software,[62] along with the TopCryst service.[63] Two structure representation approaches for rod-MOF are herein applied to get the topological description of the crystal structure: Points of Extension and Metals (PE&M) and Straight-rod representation (STR).[53] The TTF core of the tetratopic $\mathbf{1}^{4-}$ is considered as a two linked 3-connected nodes, according to the IUPAC recommendations.[64] The PE&M representation leads to the 3,3,4-coordinated underlying net of the **sqc1121** topological type (**Figure 3a, 3b**). The rods are herein a succession of vertex connected 4-membered rings, thus forming a ribbon-of-rings.

In order to obtain a straight-rod representation instead of vertex connected 4-membered rings, dummy nodes are added at the centre of each square and connected to the nearby points of extension (the carbon atoms of the –COO chelating groups). The unnecessary bonds between PEs are deleted, and after simplification the rods appear as a straight line of 4-coordinated dummy nodes (**Figure 3**). Each of them is linked to two nodes representing two different ligands, and to two other dummy nodes from the rod. The 3,4-coordinated net obtained in such way corresponds to the **tfo** topological type (**Figure 3c, 3d**).

The TopCryst service contains data on the representatives of different topological types. The nets stored in the service are obtained using the automatic procedures, which guarantees rigour of the analysis and the coverage of the large amount of data. One must nevertheless pay attention for some MOF representation with the STR description, which usually requires user intervention in an *ad hoc* manner. Therefore, for the search of the analogous rod-net MOFs a workaround is herein employed. First, the so-called standard representation that hide the rod picture is computed. This representation is indeed possible for any structure, and hence such information is collected in the TopCryst database. The 4,8-**flu** topological type is obtained. This net corresponds to the standard representation for **1-Zn_2**, in which metal atoms (coordinated by four carboxylate) and ligand's centre of mass (coordinating 8 Zn atoms via each oxygen of the four carboxylate) serve as network nodes. TopCryst reveals 116 structures with the 4,8-**flu** underlying net. Further analysis of these structures looking for rod-MOF reveals six compounds with the **sqc1121** net topology in the PE&M

representation (**see Table S2**).[65–70] Out of these, 3 structures do not display any solvent accessible voids,[65,67,70] and only one retains porosity (216 m^2/g) after evacuation.[68]

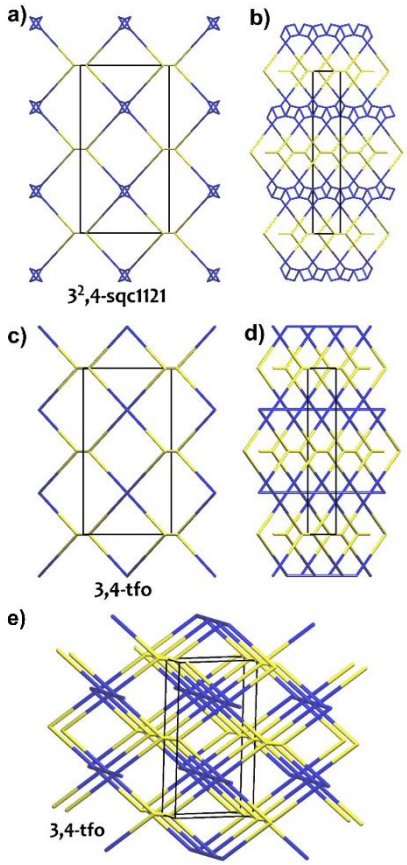

Figure 3. The PE&M representation of the **1-Zn_2** leads to underlying net **sqc1121** with rods represented as a chain of vertex connected 4-membered rings as shown down to [100] (a) and [001] (b) directions. The corresponding straight rod representation leads to underlying net **tfo** shown down to [100] (c) and [001] (d) directions, and e) close view of the rods in the straight-rod representation for **1-Zn_2**.

The material stability towards solvent exchange and drying was investigated by infrared spectroscopy and powder X-ray diffraction (PXRD). The diffraction pattern of the as-synthesized sample is in accordance with the simulated one. The larger peak at 17° may be due to preferential orientation of the crystallites. Upon successive washings with acetone and drying, infrared spectroscopy shows the disappearance of most of the DMAc signal (peak at 1630 cm^{-1}) and the appearance of peaks related to acetone (*e.g.* at 1708 cm^{-1}) (**see Fig. S8**). According to PXRD, the frameworks retains its crystallinity (**see Fig. S2**). These observations suggest that pores content can be easily exchanged without any major modification of the structure. The acetone-exchanged solid was exposed to nitrogen sorption experiments at 77 K after activation at various temperature (30, 70 and 120°C). Whatever the temperature of activation, no significant accessible microporosity was detected (deduced Brunauer–Emmett–Teller surface area reach 17, 14 and 12 m^2/g, respectively). This suggests that the structure

collapses upon complete removal of the solvent. Exposure of the material to DMAc solvent after evacuation did not restore the crystallinity (**see Fig. S4**).

Conductivity measurements on compressed-pellets of **1-Zn$_2$** reveal that the non-oxidised powder has a room-temperature conductivity of 2 to $3 \cdot 10^{-7}$ S·m^{-1}. It is common for TTF based CP to be oxidised post-synthetically in order to increase the conductivity values. The **1-H$_4$** ligand has redox potential similar to pristine TTF ($E_{1/2}$ = 0.29 and 0.51 V vs Fc^+/Fc) and therefore matches the I_2/I_3^- couple potentials (**see Fig. S1**). While direct exposure of the crystals to iodine vapours destroyed the crystallinity, immersion of the **1-Zn$_2$** powder in an iodine solution in $CHCl_3$ (0.05M) promotes in milder conditions the oxidation of the TTF core. Elemental analysis and Raman spectroscopy displays the presence of I_3^- and I_5^- (see below). PXRD shows that the solid remains crystalline after exposure to I_2 with minor structure changes, supporting the fact that the cavities are accessible to guests (**see Fig. S4**). After oxidation, the conductivity value rises up to $5.5 \cdot 10^{-4}$ S·m^{-1} on one sample (median value $2.7 \cdot 10^{-4}$ S·m^{-1} out of 4 measurements). A rapid decay over 2 to 3 hours is observed, with a complete return to the initial σ values after 72 hours at RT. The conductivity is restored again through exposure to I_2 in similar conditions. This is probably indicative of the release of I_2 and the restoration of the initial non-oxidised CP.

The ligand **1-H$_4$** is characterized by the tetrathiafulvalene (TTF) core, which usually has a high electron density in TTF-based molecules. The frontier orbitals for **1-H$_4$** calculated by DFT show, as expected, a charge density mostly concentrated on the TTF core, both in the case of the neutral (**Figure 4**, left panel) and the radical cation (**Figure 4**, right panel). Therefore, selected charge-sensitive vibrational modes bound to the TTF core observed in the Raman spectra can be used to estimate the oxidation states of **1-H$_4$** and also in the case of the derived materials **1-Zn$_2$** and **1-Zn$_2$-I$_2$**, with the same TTF core. In particular, the stretching C=C mode characterized by a strong linear frequency dependence on charge,[71,72] observed in the 1400 - 1600 cm^{-1} frequency range, is widely used in the case of BEDT-TTF salts [73] and other TTF-based solids.[74] This method is known to be a very sensitive microscopic tool for charge estimation due to the energy scale used.

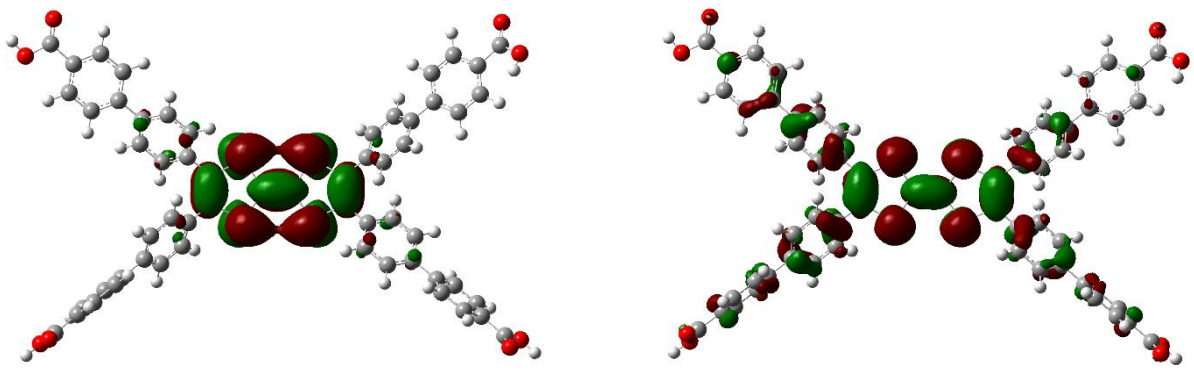

Figure 4. Frontier molecular orbitals: HOMO (Highest Occupied Molecular Orbital) of the neutral **1-H$_4$** (left), and SOMO (Single Occupied Molecular Orbital) of the **1-H$_4^{\bullet+}$** radical cation (right), calculated by DFT methods.

Figure 5 in the lower panel shows the vibrational pattern of the charge-sensitive stretching C=C mode labeled as ν_c, localized on the TTF core both in the neutral **1-H$_4$** (left) and in the **1-H$_4^{\bullet+}$** radical cation (right). ν_C affects the central C=C bond and the two wing C=C bonds in the neutral **1-H$_4$**, but only the central C=C bond in the **1-H$_4^{\bullet+}$** radical cation, the difference in the mode pattern being related to the shape of the TTF core, which is bent for the neutral and flat for the cation (see top panel in Fig. 6).

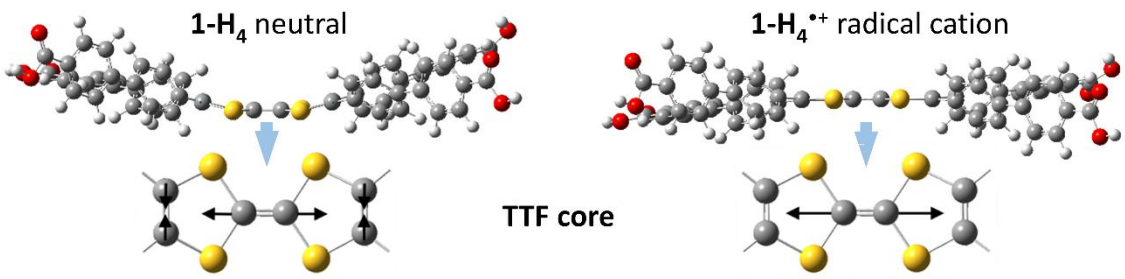

Figure 5. The side view and the vibration pattern of the charge-sensitive C=C stretching ν_c mode of the neutral **1-H$_4$** (left), and the **1-H$_4^{\bullet+}$** radical cation (right), based on the DFT calculations.

The room temperature Raman spectra of **1-H$_4$**, **1-Zn$_2$**, and **1-Zn$_2$-I$_2$**, in the frequency range of the stretching C=C vibrations are shown in **Figure 6**, together with the theoretical Raman spectra of **1-H$_4$**, and the **1-H$_4^{\bullet+}$**. The ν_c mode is shown as a strong band centered at 1392 cm^{-1} in the theoretical spectrum of the cation (ν_c^{+1}), while it appears as a very weak feature located at 1580 cm^{-1} in the spectrum of the neutral (ν_c^{0}), close to the stronger C=C stretching band at 1595 cm^{-1} of the molecular wings ($\nu_{C=C\ wing}$) (**Fig. 7b**). The frequency difference of the ν_c mode upon oxidation of **1-H$_4$** is about 190 cm^{-1}, but the proximity of another C=C stretching feature may make the ν_c^{0} assignment ambiguous.

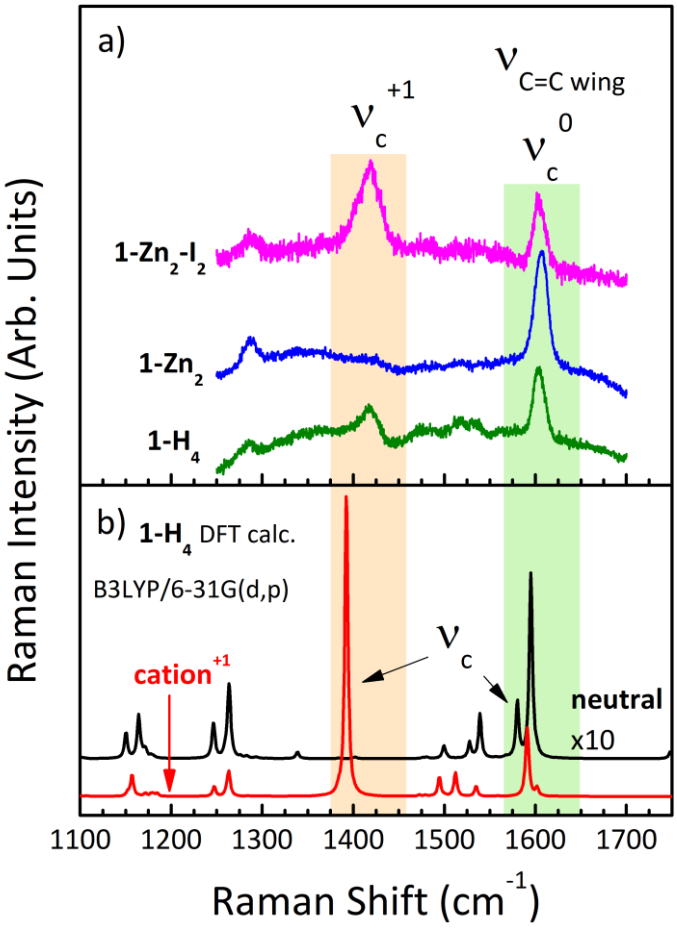

Figure 6. (a) Raman spectra of **1-H$_4$**, **1-Zn$_2$**, and **1-Zn$_2$-I$_2$**, in the frequency range of the C=C stretching vibrations, recorded at room temperature with the 632.8 nm excitation line. The spectra show the charge-sensitive ν_c mode related to the neutral molecules (ν_c^0) and to the cations with charge +1*e*; (b) theoretical Raman spectra of the isolated **1-H$_4$** molecule, both the neutral and the cation, calculated at the B3LYP/6-31G(d,p) level of theory; the neutral **1-H$_4$** spectrum have been multiplied by a factor of 10. The spectra in both panels are offset for clarity.

Thus, we assign a broad feature at ~1600 cm^{-1} in the experimental Raman spectra of **1-H$_4$**, **1-Zn$_2$**, and **1-Zn$_2$-I$_2$**, as the sum of ν_c^0 and some of the $\nu_{C=C\ wing}$ modes, generally related to both the neutral and the cation (**Table 1**). It is worth noting that the presence of the neutral ν_c^0 feature is expected in all the experimental spectra, since **1-H$_4$** and **1-Zn$_2$** are nominally neutral, and neutral molecules are most likely present in the oxidized **1-Zn$_2$-I$_2$**. The strong feature at ~1420 cm^{-1} attributed to the ν_c^{+1} mode of the cation is clearly seen in the experimental spectrum of **1-Zn$_2$-I$_2$**, as expected, and also for **1-H$_4$** (**Table 1**). Given the two orders of magnitude higher intensity of the ν_c mode in the theoretical spectrum of the cation compared to the neutral, the experimental Raman spectra of **1-Zn$_2$-I$_2$** and **1-H$_4$** suggest that relatively small amounts of molecules are oxidized in both materials. For **1-Zn$_2$-I$_2$**, this is probably due to the release of iodine during the experiment. The presence of I_3^- and I_5^- was also confirmed with the characteristic polyiodide vibrations in the 110-160 cm^{-1} range (**see Fig. S7**).[75,76]

Table 1. The position in cm^{-1} of the charge-sensitive C=C stretching ν_c mode of **1-H$_4$** for the neutral ν_c^0 plus $\nu_{C=C\ wing}$, and the cation ν_c^{+1}, in experimental Raman spectra of **1-H$_4$**, **1-Zn$_2$**, and **1-Zn$_2$-I$_2$**, and calculated (DFT) Raman spectra of **1-H$_4$**.

	$\nu_c^0/\nu_{C=C\ wing}$	ν_c^{+1}
1-H$_4$	~1603	1419
1-Zn$_2$	~1607	-
1-Zn$_2$-I$_2$	~1604	1418
1-H$_4$ (DFT)[a]	1580	1392

[a]Theory level: B3LYP/6-31G(d,p), scaled with a 0.9614 factor.

Conclusion

The extension of the ubiquitous TTFTB scaffold using biphenyl arms is described. This novel **1-H$_4$** ligand presents a *ca.* 50% size extension related to the parent TTFTB. Its combination with Zn(II) provided a rod based coordination polymer presenting large potential voids in SCXRD, as expected from the extended ligand structure. The TTF cores stack along 1-D chains without dimerization or trimerization, but the shortest intermolecular S-S distances over 4.0 Å prevents band-like charge transport. Although no permanent porosity was observed by nitrogen sorption experiments after full activation, solvent exchange was successful, indicating that the porosity must be accessible. Treatment of this material with iodine shows an increase of the conductivity by *ca.* 3 orders of magnitude. Current works are ongoing to expand the scaffold types of ligands used for through space pathway conductive CP, or using metals with a higher degree of oxidation to further stabilize the CPs after evacuation.

Experimental part

General procedures

All the solvents and precursors were commercially available and used without further purification. ^{1}H and ^{13}C spectra were recorded on a Bruker Advance DRX 300 spectrometer operating at 300 MHz for ^{1}H and 76 MHz for ^{13}C, or on a Bruker Advance DRX 500 operating at 500 MHz for ^{1}H and 125 MHz for ^{13}C. Chemical shifts are given in ppm relative to tetramethylsilane TMS and coupling constants *J* in Hz. The residual non-deuterated solvent was used as an internal standard. Mass spectra were obtained by the MALDI-TOF techniques by using a Bruker Biflex-III-TM apparatus, equipped with a 337 nm N_2

laser. Methyl 4-(4-bromophenyl)benzoate and tetrathiafulvalene were purchased from Sigma Aldrich chemicals and used as received.

Raman measurements. Typical dimensions of the single crystalline samples used in the Raman measurements were between 0.5 and 1 mm (about $0.5\times0.5\times0.5$ mm^3). Raman spectra were measured in a backward scattering geometry using a Raman LABRAM HR800 spectrometer equipped with a microscope and He-Ne laser excitation λ = 632.8 nm. The spectra were recorded at room temperature with a spectral resolution of 2 cm^{-1} and power reduced to approximately 0.3 mW to avoid sample overheating.

DFT. Density functional theory (DFT) calculations of the charge density and normal vibrations of the isolated 1-H4 molecule, the neutral and the radical cation, were performed with Gaussian 09,[77] using the 6-31G(d,p) basis set and the hybrid density functional (B3LYP). The result of the structure optimization corresponds to energy minima, as no imaginary frequencies were found. Based on the optimized structure, vibrational frequencies and Raman scattering activities were calculated. The frequencies obtained with a quantum harmonic oscillator approximation tend to be higher than the experimental ones, therefore the scaling factor of 0.9614 was applied to the calculated frequencies.[78] The theoretical Raman intensities were calculated from the scattering activities and wavenumbers using the described procedures.[79,80] The DFT-calculated Raman spectra were generated using the GaussSum program.[81]

X-Ray structure determinations

Details about data collection and solution refinement are given in Table S1. Data collections were performed on a Rigaku Oxford Diffraction SuperNova diffractometer equipped with an Atlas CCD detector and micro-focus Cu-K_α radiation (λ = 1.54184 Å). The structures were solved by intrinsic phasing and refined on F^2 by full matrix least-squares techniques with SHELX programs (SHELXT 2018/2 and SHELXL 2018/3)[82,83] using the ShelXle and the Olex2 graphical user interfaces.[58,84] All non-H atoms were refined anisotropically and absorption was corrected by multiscan empirical absorption using spherical harmonics with CrysAlisPro program. The H atoms were placed at calculated positions and refined using a riding model. Crystallographic data for the two structures have been deposited with the Cambridge Crystallographic Data Centre, deposition numbers CCDC 2300287 for **1-Me$_4$**, 2300286 for **1-Zn$_2$**. These data can be obtained free of charge from CCDC, 12 Union road, Cambridge CB2 1EZ, UK (e-mail: deposit@ccdc.cam.ac.uk or http://www.ccdc.cam.ac.uk).

Compressed-pellet conductivity measurements

Electrical conductivity measurements at room temperature were performed in two points on *ca.* 1 cm wide and 30 µm thick compressed pellets (8 bars). Gold wires were glued with silver paste on one face of the pellets as parallel strips 1 to 2 mm apart. We have used a Keithley 486 picoammeter to apply a constant voltage (up to 30V) and measure the current, leading to resistance values up to 100GΩ.

Nitrogen sorption experiments

The nitrogen sorption experiments at 77 K were carried out using a Micromeritics Triflex volumetric adsorption apparatus. The sample (~20 mg) was activated under vacuum at various temperatures (30, 70 and 120°C) for few hours prior to the sorption measurement.

Synthesis

Tetrakis(4-carboxylate methyl ester biphenyl)tetrathiafulvalene (1-Me$_4$). $Pd(OAc)_2$ (17 mg, 75 µmol, 0.26 equiv.), P(*t*Bu_3)·HBF_4 (68 mg, 0.23 mmol, 0.8 equiv.) and Cs_2CO_3 (1.04 g, 3.2 mmol, 11 equiv.) were added in a dry Schlenk flask under Argon. Dry and degassed 1,4-dioxane (6 mL) was added and the mixture was heated at 90°C for 15 minutes. TTF (59 mg, 0.29 mmol, 1 equiv.) and methyl 4-(4-bromophenyl)benzoate (0.50 g, 1.72 mmol, 6 equiv.) were added, the flask was degassed again, and the mixture was refluxed for 4 days. The mixture was diluted with $CHCl_3$ (6 mL) and filtered on Celite, and the residue wash with portions of $CHCl_3$. The filtrate was evaporated to dryness, and the compound was purified by column chromatography (SiO_2, CH_2Cl_2/THF/NEt_3 100/0/0.2 to 95/5/0.2) and recrystallization from CH_2Cl_2/MeOH, to yield **1-Me$_4$** as a red solid (236 mg, 79%).

^{1}H NMR ($CDCl_3$, 300 MHz): δ = 8.09 (d, J = 8.5 Hz, 8 H), 7.63 (d, J = 8.5 Hz, 8 H), 7.54 (d, J = 8.2 Hz, 8 H), 7.37 (d, J = 8.2 Hz, 8 H), 3.94 (s, 12 H).

LRMS (MALDI): m/z = 1044.4 , theor. 1044.2 (M^+).

Elemental analysis : exp. %C 63.77, %H 4.11, %S 10.61 ; th. (1-Me_4, 6 H_2O) %C 64.57, %H 4.89, %S 11.12

Tetrakis(4-carboxylic acid biphenyl)tetrathiafulvalene (1-H$_4$). 1-Me$_4$ (236 mg, 0.23 mmol, 1 equiv.) was dissolved in THF/MeOH (1/1 %v/%v ; 20 mL) and a solution of NaOH (0.28 g, 6.9 mmol, 30 equiv.) in H_2O (4 mL) was added. After a 48 h. reflux, H_2O was added (*ca.* 100 mL) followed by HCl 10% until pH = 1 was reached. The red precipitate was filtered on sintered glass funnel, washed with H_2O (20 mL) and dried under reduced pressure (206 mg, 92 %).

^{1}H NMR (DMSO-d_6, 300 MHz): δ = 8.00 (d, J = 8.4 Hz, 8 H), 7.80 (d, J = 8.4 Hz, 8 H), 7.75 (d, J = 8.2 Hz, 8 H), 7.40 (d, J = 8.2 Hz, 8 H).

^{13}C NMR (DMSO-d_6, 125 MHz): δ = 166.98, 143.06, 139.34, 129.95, 129.53, 127.47, 126.76.

HRMS (MALDI): m/z = 988.12727 , theor. 988.12875 (M^+).

Elemental analysis : exp. %C 63.45, %H 4.12, %S 10.63 ; th. (1-H_4, 6 H_2O) %C 63.49, %H 4.41, %S 11.69.

Synthesis of the coordination polymer 1-Zn_2

Method A. *Preparation of single crystals.* **1**-**H_4** (1 mg, 1 μmol, 1 equiv) was dissolved in DMAc (3 mL) in a 5 mL Teflon lined cell for autoclave (internal diameter *ca*. 1cm). A solution of $Zn(NO_3)_2$, $6H_2O$ (0.6 mg, 2 μmol, 2 equiv) in EtOH (0.5 mL) was carefully layered and the autoclave was sealed. After applying a specific heating protocol (25°C to 100°C at 6.25°C/h. – 100°C for 72 h. – 100°C to 25°C at 7.5°C/h.), dark red needle crystals of **1-Zn_2** were obtained.

Method B. *Large scale synthesis of microcrystalline powder.* **1**-**H_4** (10 mg, 10 μmol, 1 equiv) was dissolved in DMAc (15 mL) in a 20 mL Teflon lined cell for autoclave (internal diameter *ca*. 2.5 cm). A solution of $Zn(NO_3)_2$, $6H_2O$ (6 mg, 20 μmol, 2 equiv) in EtOH (2.5 mL) was added and the autoclave was sealed. After applying a specific heating protocol (25°C to 100°C at 6.25°C/h. – 100°C for 72 h. – 100°C to 25°C at 7.5°C/h.), a microcrystalline powder of **1-Zn_2** was obtained. From 8 autoclaves (80 mg of **1-H_4**), 30 mg of **1-Zn_2** are obtained after filtration on paper and portion-wise washings with DMAc (33% yield).

The crystals were further characterized with single-crystal X-ray diffraction and PXRD analysis.

Post-synthetic oxidation of 1-Zn_2. 10 mg of **1-Zn_2** were suspended in a solution of I_2 in $CHCl_3$ (0.05 M, 5 mL). After 5 hours, the supernatant was removed and the powder washed with $CHCl_3$ (3 x 5 mL).

Elemental analysis : exp. %C 30.02, %H 2.46, %N 1.43, %S 5.59 ; th. (1-Zn_2, $(I_3^-)_{0.5}$, $(I_5^-)_{0.5}$, 2(C_5H_7NO), 8($CHCl_3$)) %C 3.34, %H 2.10, %N 1.08, %S 4.94.

Acknowledgements

This work was supported in France by the CNRS, the University of Angers and the ANR (JCJC PANDEMIC). N.A. and I.O. thank the Narodowa Agencja Wymiany Akademickiej – NAWA (Poland, BPN/BFR/2021/1/00001/U/00001) and the French Ministry of Foreign Affairs and the French Ministry of Education and Research (France, PHC Project 48119PG) for financial support through the bilateral Polonium project. The work in Poland was supported within the Statutory Activities of the Institute of Molecular Physics Polish Academy of Sciences. The Authors are grateful to Dr. Adam Mizera (Inst. of Molecular Physics, Polish Acad. Sci.) for technical assistance in DFT calculations. P.N.Z. and D.M.P.

thank the MUR for the grant PRIN2020 “Nature Inspired Crystal Engineering (NICE)” and Prof. Vladislav A. Blatov at the Samara Center for Theoretical Materials Science for providing the free ToposPro software (https://topospro.com). Prof. Enric Canadell is warmly acknowledged for his valuable comments.

References

1 S. R. Batten, N. R. Champness, X.-M. Chen, J. Garcia-Martinez, S. Kitagawa, L. Öhrström, M. O’Keeffe, M. P. Suh and J. Reedijk, *Pure Appl. Chem.*, 2013, **85**, 1715–1724.
2 B. F. Hoskins and R. Robson, *J. Am. Chem. Soc.*, 1990, **112**, 1546–1554.
3 B. F. Abrahams, B. F. Hoskins and R. Robson, *J. Am. Chem. Soc.*, 1991, **113**, 3606–3607.
4 A. C. Sudik, A. R. Millward, N. W. Ockwig, A. P. Côté, J. Kim and O. M. Yaghi, *J. Am. Chem. Soc.*, 2005, **127**, 7110–7118.
5 F. Gándara, H. Furukawa, S. Lee and O. M. Yaghi, *J. Am. Chem. Soc.*, 2014, **136**, 5271–5274.
6 Y. Peng, V. Krungleviciute, I. Eryazici, J. T. Hupp, O. K. Farha and T. Yildirim, *J. Am. Chem. Soc.*, 2013, **135**, 11887–11894.
7 K. Ohara, M. Kawano, Y. Inokuma and M. Fujita, *J. Am. Chem. Soc.*, 2010, **132**, 30–31.
8 Y.-B. Huang, J. Liang, X.-S. Wang and R. Cao, *Chem. Soc. Rev.*, 2017, **46**, 126–157.
9 G. Mouchaham, B. Abeykoon, M. Gimenez-Marques, S. Navalon, A. Santiago-Portillo, M. Affram, N. Guillou, C. Martineau, H. Garcia, A. Fateeva and T. Devic, *Chem. Commun.*, 2017, **53**, 7661–7664.
10 J.-R. Li, J. Sculley and H.-C. Zhou, *Chem. Rev.*, 2012, **112**, 869–932.
11 G. Ferey, C. Serre, T. Devic, G. Maurin, H. Jobic, P. L. Llewellyn, G. De Weireld, A. Vimont, M. Daturi and J.-S. Chang, *Chem. Soc. Rev.*, 2011, **40**, 550–562.
12 T. Duerinck and J. F. M. Denayer, *Chem. Eng. Sci.*, 2015, **124**, 179–187.
13 J. Navarro-Sánchez, A. I. Argente-García, Y. Moliner-Martínez, D. Roca-Sanjuán, D. Antypov, P. Campíns-Falcó, M. J. Rosseinsky and C. Martí-Gastaldo, *J. Am. Chem. Soc.*, 2017, **139**, 4294–4297.
14 N. Zigon, M. Hoshino, S. Yoshioka, Y. Inokuma and M. Fujita, *Angew. Chem.*, 2015, **54**, 9033–9037.
15 Y. Inokuma, S. Yoshioka, J. Ariyoshi, T. Arai, Y. Hitora, K. Takada, S. Matsunaga, K. Rissanen and M. Fujita, *Nature*, 2013, **495**, 461–466.
16 Y. Inokuma, S. Yoshioka, J. Ariyoshi, T. Arai, Y. Hitora, K. Takada, S. Matsunaga, K. Rissanen and M. Fujita, *Nature*, 2013, **501**, 262–262.
17 S. Lee, E. A. Kapustin and O. M. Yaghi, *Science*, 2016, **353**, 808–811.
18 K. A. McDonald, S. Seth and A. J. Matzger, *Cryst. Growth Des.*, 2015, **15**, 5963–5972.
19 A. Douvali, A. C. Tsipis, S. V. Eliseeva, S. Petoud, G. S. Papaefstathiou, C. D. Malliakas, I. Papadas, G. S. Armatas, I. Margiolaki, M. G. Kanatzidis, T. Lazarides and M. J. Manos, *Angew. Chem. Int. Ed.*, 2015, **54**, 1651–1656.
20 I. Stassen, N. Burtch, A. Talin, P. Falcaro, M. Allendorf and R. Ameloot, *Chem. Soc. Rev.*, 2017, **46**, 3185–3241.
21 L. S. Xie, G. Skorupskii and M. Dincă, *Chem. Rev.*, 2020, **120**, 8536–8580.
22 L. R. Melby, R. J. Harder, W. R. Hertler, W. Mahler, R. E. Benson and W. E. Mochel, *J. Am. Chem. Soc.*, 1962, **84**, 3374–3387.
23 A. Aumüller, P. Erk, G. Klebe, S. Hünig, J. U. von Schütz and H.-P. Werner, *Angew. Chem. Int. Ed.*, 1986, **25**, 740–741.
24 A. Nafady, A. P. O’Mullane and A. M. Bond, *Coord. Chem. Rev.*, 2014, **268**, 101–142.
25 S. Takaishi, M. Hosoda, T. Kajiwara, H. Miyasaka, M. Yamashita, Y. Nakanishi, Y. Kitagawa, K. Yamaguchi, A. Kobayashi and H. Kitagawa, *Inorg. Chem.*, 2009, **48**, 9048–9050.
26 Y. Kobayashi, B. Jacobs, M. D. Allendorf and J. R. Long, *Chem. Mater.*, 2010, **22**, 4120–4122.
27 D. L. Turner, T. P. Vaid, P. W. Stephens, K. H. Stone, A. G. DiPasquale and A. L. Rheingold, *J. Am. Chem. Soc.*, 2008, **130**, 14–15.

28 T. L. A. Nguyen, R. Demir-Cakan, T. Devic, M. Morcrette, T. Ahnfeldt, P. Auban-Senzier, N. Stock, A.-M. Goncalves, Y. Filinchuk, J.-M. Tarascon and G. Férey, *Inorg. Chem.*, 2010, **49**, 7135–7143.
29 L. Liu, Y. Zhou, S. Liu and M. Xu, *ChemElectroChem*, 2018, **5**, 6–19.
30 Y. Zhou, Q. Hu, F. Yu, G.-Y. Ran, H.-Y. Wang, N. D. Shepherd, D. M. D'Alessandro, M. Kurmoo and J.-L. Zuo, *J. Am. Chem. Soc.*, 2020, **142**, 20313–20317.
31 K. J. Erickson, F. Léonard, V. Stavila, M. E. Foster, C. D. Spataru, R. E. Jones, B. M. Foley, P. E. Hopkins, M. D. Allendorf and A. A. Talin, *Adv. Mater.*, 2015, **27**, 3453–3459.
32 Y. Ren, G. H. Chia and Z. Gao, *Nano Today*, 2013, **8**, 577–597.
33 H. Banda, J.-H. Dou, T. Chen, N. J. Libretto, M. Chaudhary, G. M. Bernard, J. T. Miller, V. K. Michaelis and M. Dincă, *J. Am. Chem. Soc.*, 2021, **5**, 2285–2292.
34 N. Gedikoglu, P. Salcedo-Abraira, L. H. B. Nguyen, N. Guillou, N. Dupré, C. Payen, N. Louvain, L. Stievano, P. Poizot and T. Devic, *J. Mater. Chem. A*, 2023, **11**, 23909–23921.
35 A. Mallick, H. Liang, O. Shekhah, J. Jia, G. Mouchaham, A. Shkurenko, Y. Belmabkhout, H. N. Alshareef and M. Eddaoudi, *Chem. Commun.*, 2020, **56**, 1883–1886.
36 M. A. Borysiewicz, J.-H. Dou, I. Stassen and M. Dincă, *Faraday Discuss.*, 2021, **231**, 298–304.
37 K. Jayaramulu, M. Horn, A. Schneemann, H. Saini, A. Bakandritsos, V. Ranc, M. Petr, V. Stavila, C. Narayana, B. Scheibe, Š. Kment, M. Otyepka, N. Motta, D. Dubal, R. Zbořil and R. A. Fischer, *Adv. Mater.*, 2021, **33**, 2004560.
38 H. Leclerc, T. Devic, S. Devautour-Vinot, P. Bazin, N. Audebrand, G. Férey, M. Daturi, A. Vimont and G. Clet, *J. Phys. Chem. C*, 2011, **115**, 19828–19840.
39 L. Sun, C. H. Hendon, M. A. Minier, A. Walsh and M. Dincă, *J. Am. Chem. Soc.*, 2015, **137**, 6164–6167.
40 N. Avarvari and J. D. Wallis, *J. Mater. Chem.*, 2009, **19**, 4061–4076.
41 F. Pop, N. Zigon and N. Avarvari, *Chem. Rev.*, 2019, **119**, 8435–8478.
42 N. Avarvari, *Eur. J. Inorg. Chem.*, 2020, **18**, 1706–1719.
43 T. L. A. Nguyen, T. Devic, P. Mialane, E. Rivière, A. Sonnauer, N. Stock, R. Demir-Cakan, M. Morcrette, C. Livage, J. Marrot, J.-M. Tarascon and G. Férey, *Inorg. Chem.*, 2010, **49**, 10710–10717.
44 T. C. Narayan, T. Miyakai, S. Seki and M. Dincă, *J. Am. Chem. Soc.*, 2012, **134**, 12932–12935.
45 M. Souto, J. Romero, J. Calbo, I. J. Vitórica-Yrezábal, J. L. Zafra, J. Casado, E. Ortí, A. Walsh and G. Mínguez Espallargas, *J. Am. Chem. Soc.*, 2018, **140**, 10562–10569.
46 D. Bechu, G. Rogez, M. W. Hosseini and S. A. Baudron, *New J. Chem.*, 2019, **43**, 14291–14298.
47 D. Bechu, L. S. Xie, N. L. Breton, S. Choua, M. Dincă, M. W. Hosseini and S. A. Baudron, *Chem. Commun.*, 2020, **56**, 2407–2410.
48 Z.-M. Yang, S.-P. Zhao, M.-H. Zhang, Z.-D. Zhang, T.-R. Ma, S. Yuan, J. Su, C.-H. Li and J.-L. Zuo, *Angew. Chem. Int. Ed.*, 2023, **62**, e202304183.
49 S. S. Park, E. R. Hontz, L. Sun, C. H. Hendon, A. Walsh, T. Van Voorhis and M. Dincă, *J. Am. Chem. Soc.*, 2015, **137**, 1774–1777.
50 L. S. Xie and M. Dincă, *Isr. J. Chem.*, 2018, **58**, 1119–1122.
51 J. Castells-Gil, S. Mañas-Valero, I. J. Vitórica-Yrezábal, D. Ananias, J. Rocha, R. Santiago, S. T. Bromley, J. J. Baldoví, E. Coronado, M. Souto and G. Mínguez Espallargas, *Chem. Eur. J.*, 2019, **25**, 12636–12643.
52 J. Su, T.-H. Hu, R. Murase, H.-Y. Wang, D. M. D'Alessandro, M. Kurmoo and J.-L. Zuo, *Inorg. Chem.*, 2019, **58**, 3698–3706.
53 L. S. Xie, E. V. Alexandrov, G. Skorupskii, D. M. Proserpio and M. Dincă, *Chem. Sci.*, 2019, **10**, 8558–8565.
54 D. Ukaj, H. Bunzen, J. Berger, G. Kieslich and R. A. Fischer, *Chem. Mater.*, 2021, **33**, 2532–2542.
55 A. Schoedel, M. Li, D. Li, M. O'Keeffe and O. M. Yaghi, *Chem. Rev.*, 2016, **116**, 12466–12535.
56 M. Eddaoudi, J. Kim, N. Rosi, D. Vodak, J. Wachter, M. O'Keeffe and O. M. Yaghi, *Science*, 2002, **295**, 469–472.
57 Y. Mitamura, H. Yorimitsu, K. Oshima and A. Osuka, *Chem. Sci.*, 2011, **2**, 2017–2021.
58 O. V. Dolomanov, L. J. Bourhis, R. J. Gildea, J. a. K. Howard and H. Puschmann, *J. Appl. Cryst.*, 2009, **42**, 339–341.

59 N. L. Rosi, J. Kim, M. Eddaoudi, B. Chen, M. O'Keeffe and O. M. Yaghi, *J. Am. Chem. Soc.*, 2005, **127**, 1504–1518.
60 A. L. Spek, *Acta Cryst C*, 2015, **71**, 9–18.
61 A. L. Spek, *Acta Cryst D*, 2009, **65**, 148–155.
62 V. A. Blatov, A. P. Shevchenko and D. M. Proserpio, *Cryst. Growth Des.*, 2014, **14**, 3576–3586.
63 A. P. Shevchenko, A. A. Shabalin, I. Yu. Karpukhin and V. A. Blatov, *Science and Technology of Advanced Materials: Methods*, 2022, **2**, 250–265.
64 C. Bonneau, M. O'Keeffe, D. M. Proserpio, V. A. Blatov, S. R. Batten, S. A. Bourne, M. S. Lah, J.-G. Eon, S. T. Hyde, S. B. Wiggin and L. Öhrström, *Cryst. Growth Des.*, 2018, **18**, 3411–3418.
65 R.-B. Fu, S.-M. Hu, H.-S. Zhang, L.-S. Wang, Y.-M. Li, X.-H. Huang and X.-T. Wu, *Jiegou Huaxue*, 2005, **24**, 1231.
66 Z. Pan, H. Zheng, T. Wang, Y. Song, Y. Li, Z. Guo and S. R. Batten, *Inorg. Chem.*, 2008, **47**, 9528–9536.
67 C.-H. Ma and Y.-S. Yan, *Acta Cryst. E*, 2009, **65**, m1555–m1555.
68 L.-L. Qu, Y.-L. Zhu, Y.-Z. Li, H.-B. Du and X.-Z. You, *Cryst. Growth Des.*, 2011, **11**, 2444–2452.
69 C. S. Hawes, N. F. Chilton, B. Moubaraki, G. P. Knowles, A. L. Chaffee, K. S. Murray, S. R. Batten and D. R. Turner, *Dalton Trans.*, 2015, **44**, 17494–17507.
70 X.-H. Zhu, X.-C. Cheng and Y.-H. Qian, *Z. Naturforsch. B*, 2017, **72**, 937–940.
71 T. Yamamoto, M. Uruichi, K. Yamamoto, K. Yakushi, A. Kawamoto and H. Taniguchi, *J. Phys. Chem. B*, 2005, **109**, 15226–15235.
72 A. Girlando, *J. Phys. Chem. C*, 2011, **115**, 19371–19378.
73 K. Yakushi, *Crystals*, 2012, **2**, 1291–1346.
74 F. Solano, P. Auban-Senzier, I. Olejniczak, B. Barszcz, T. Runka, P. Alemany, E. Canadell, N. Avarvari and N. Zigon, *Chem. Eur. J.*, 2023, **29**, e202203138.
75 P. H. Svensson and L. Kloo, *Chem. Rev.*, 2003, **103**, 1649–1684.
76 I. Jerman, V. Jovanovski, A. Šurca Vuk, S. B. Hočevar, M. Gaberšček, A. Jesih and B. Orel, *Electrochim. Acta*, 2008, **53**, 2281–2288.
77 Gaussian 09 (Revision D.01), M. J. Frisch, G. W. Trucks, H. B. Schlegel, G. E. Scuseria, M. A. Robb, J. R. Cheeseman, G. Scalmani, V. Barone, B. Mennucci, G. A. Petersson, H. Nakatsuji, M. Caricato, X. Li, H. P. Hratchian, A. F. Izmaylov, J. Bloino, G. Zheng, J. L. Sonnenberg, M. Hada, M. Ehara, K. Toyota, R. Fukuda, J. Hasegawa, M. Ishida, T. Nakajima, Y. Honda, O. Kitao, H. Nakai, T. Vreven, J. A. Montgomery, Jr., J. E. Peralta, F. Ogliaro, M. Bearpark, J. J. Heyd, E. Brothers, K. N. Kudin, V. N. Staroverov, T. Keith, R. Kobayashi, J. Normand, K. Raghavachari, A. Rendell, J. C. Burant, S. S. Iyengar, J. Tomasi, M. Cossi, N. Rega, J. M. Millam, M. Klene, J. E. Knox, J. B. Cross, V. Bakken, C. Adamo, J. Jaramillo, R. Gomperts, R. E. Stratmann, O. Yazyev, A. J. Austin, R. Cammi, C. Pomelli, J. W. Ochterski, R. L. Martin, K. Morokuma, V. G. Zakrzewski, G. A. Voth, P. Salvador, J. J. Dannenberg, S. Dapprich, A. D. Daniels, O. Farkas, J. B. Foresman, J. V. Ortiz, J. Cioslowski, and D. J. Fox, Gaussian, Inc., Wallingford CT, 2013, .
78 A. P. Scott and L. Radom, *J. Phys. Chem.*, 1996, **100**, 16502–16513.
79 D. Michalska and R. Wysokiński, *Chem. Phys. Lett.*, 2005, **403**, 211–217.
80 R. Sun, J. Yao, S. Li and R. Gu, *Vib. Spectrosc.*, 2008, **47**, 38–43.
81 N. M. O'boyle, A. L. Tenderholt and K. M. Langner, *J. Comput. Chem.*, 2008, **29**, 839–845.
82 G. M. Sheldrick, *Acta Crystallogr. A*, 2008, **64**, 112–122.
83 G. M. Sheldrick, *Acta Crystallogr. A*, 2015, **71**, 3–8.
84 C. B. Hübschle, G. M. Sheldrick and B. Dittrich, *J. Appl. Cryst.*, 2011, **44**, 1281–1284.